ORIGINAL ARTICLE

Cytometry
PART A
Journal of the International Society for Advancement of Cytometry

Iterative H-Minima-Based Marker-Controlled Watershed for Cell Nucleus Segmentation

Can Fahrettin Koyuncu,[1] Ece Akhan,[2] Tulin Ersahin,[3] Rengul Cetin-Atalay,[3] Cigdem Gunduz-Demir[1,4]*

[1]Computer Engineering Department, Bilkent University, Ankara, TR-06800, Turkey

[2]Molecular Biology and Genetics Department, Bilkent University, Ankara, TR-06800, Turkey

[3]Medical Informatics Department, Graduate School of Informatics, Middle East Technical University, Ankara, TR-06800, Turkey

[4]Neuroscience Graduate Program, Bilkent University, Ankara, TR-06800, Turkey

Received 3 June 2015; Revised 26 October 2015; Accepted 11 January 2016

*Correspondence to: Cigdem Gunduz-Demir, Computer Engineering Department, Bilkent University, TR-06800, Ankara, Turkey.
E-mail: gunduz@cs.bilkent.edu.tr

Published online 4 March 2016 in Wiley Online Library (wileyonlinelibrary.com)

DOI: 10.1002/cyto.a.22824

Abstract

Automated microscopy imaging systems facilitate high-throughput screening in molecular cellular biology research. The first step of these systems is cell nucleus segmentation, which has a great impact on the success of the overall system. The marker-controlled watershed is a technique commonly used by the previous studies for nucleus segmentation. These studies define their markers finding regional minima on the intensity/gradient and/or distance transform maps. They typically use the h-minima transform beforehand to suppress noise on these maps. The selection of the h value is critical; unnecessarily small values do not sufficiently suppress the noise, resulting in false and oversegmented markers, and unnecessarily large ones suppress too many pixels, causing missing and undersegmented markers. Because cell nuclei show different characteristics within an image, the same h value may not work to define correct markers for all the nuclei. To address this issue, in this work, we propose a new watershed algorithm that iteratively identifies its markers, considering a set of different h values. In each iteration, the proposed algorithm defines a set of candidates using a particular h value and selects the markers from those candidates provided that they fulfill the size requirement. Working with widefield fluorescence microscopy images, our experiments reveal that the use of multiple h values in our iterative algorithm leads to better segmentation results, compared to its counterparts. © 2016 International Society for Advancement of Cytometry

Key terms

nucleus segmentation; h-minima transform; watershed; fluorescence microscopy imaging

Molecular cellular biology research has extensively used high-throughput screening for therapeutic drug discovery as it facilitates systematically conducting a series of experiments to evaluate the effectiveness of a drug. Although there are analysis tools from drug treated samples during therapeutic drug discovery, there is a need for improvement, particularly for the cases including overlayered cells for which these tools fail and users prefer manual analyses. For the development of an automated imaging tool, the first step is typically cell nucleus segmentation, which is critical for the success of the overall system.

In the literature, there exist several algorithms developed for cell nucleus segmentation. The first group of these algorithms focus on cells that are grown in monolayer in the plate and nuclei of which appear as isolated in the image. The other group consider cells grown in overlayers, on top of each other, in the plate. These overlayered cells could be less-confluent, where some overlaps appear along the boundaries of their nuclei, or more-confluent, where the nuclei appear as clusters in the image (Fig. 1). The segmentation algorithms usually start with separating foreground nucleus pixels from background, using techniques such as thresholding (1,2) and clustering (3–5). Although it is sufficient to find connected components on the

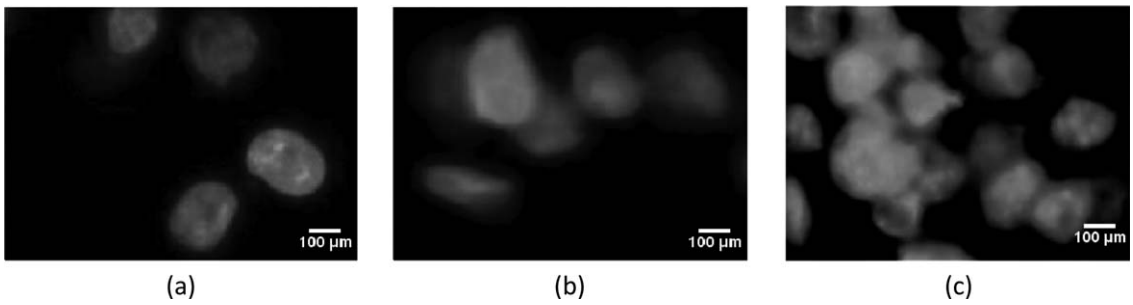

Figure 1. Example images of cells. (**a**) Monolayer cells whose nuclei appear as isolated, (**b**) less-confluent cells for which some overlaps appear along the boundaries of their nuclei, and (**c**) more-confluent cells whose nuclei appear as clusters.

foreground pixels for isolated nucleus segmentation, more advanced techniques are necessary to segment confluent cell nuclei. These include model-based segmentation algorithms and marker-controlled watersheds.

Model-based segmentation algorithms decompose clustered nuclei into individual ones by constructing their models to reflect the morphological properties of nuclei. For example, they may employ the information that nuclei are round and convex and their boundaries are radially symmetrical. A group of these algorithms have used ellipse fitting (2), Gaussian mixtures (6), and physical deformable models (7) to decompose clustered cell nuclei based on their roundness. Another group have proposed to find concave points on cluster boundaries and split the cluster from these points (8,9). As they mainly model morphological properties of nuclei, these algorithms are susceptible to undersegmentations when cells form big clusters. Voting-based algorithms have got pixels iteratively voted along the radial and tangential directions, specified by voting kernels, and considered those with larger votes as nucleus centers (10–12). Because the voting kernels are initialized using the gradient information, these algorithms lead to oversegmentations when there exist intensity variations within cell nuclei.

The marker-controlled watershed is another technique that previous algorithms have commonly used to segment clustered cell nuclei. It defines a set of markers on an image and obtains cell nucleus regions growing them only from these predefined markers. In this technique, it is crucial to correctly identify the markers since a nucleus cannot be segmented if a marker is not defined for it. The majority of the previous algorithms take regional minima found on the intensity/gradient (1) and/or the distance transform (13) maps as the markers. However, this is very sensitive to noise, and hence, may lead to defining spurious markers. To alleviate this problem, these algorithms typically apply the h-minima transform, which suppresses all minima under a value of h, before finding the regional minima (14–16). The selection of the h value directly affects the defined markers. Smaller h values do not sufficiently suppress the noise, which might result in defining false and oversegmented markers. On the other hand, larger h values suppress too many pixels such that minima become connected to each other or to the background; this might yield missing and undersegmented markers.

The previous algorithms typically use the same h value for an entire image or for each connected component of the binary mask of the image, which corresponds to a nucleus cluster. They select this h value experimentally (14,17) or by optimizing a criterion function (16). Once it is selected, this value is used for the entire image or the corresponding connected component. On the other hand, the same image/component may require using different h values for more accurately identifying the markers. For instance, Figure 2 shows the markers found on an example image using three different h values. The cell nuclei illustrated as red markers in Figure 2b can only be identified using a smaller h value. However, the same h value yields many oversegmented cell nuclei, markers of which are shown in magenta in Figures 2b and 2c. Increasing the h value may overcome the oversegmentation problem, but this time, it may cause undersegmentations, as illustared with a yellow marker in Figure 2d, and missing nuclei.

In this article, we propose a new marker-controlled watershed algorithm to address this issue. To this end, the proposed algorithm iteratively identifies its markers, considering a set of different h values. In each iteration, it defines a set of candidates using a particular h value and selects the markers from those candidates provided that they fulfill the size requirement. In the literature, there also exist h-minima based methods that make use of iterative approaches to identify their markers (15,16). After identifying the initial markers using a selected h value, Cheng and Rajapakse refine the shape of these markers by increasing the selected h value iteratively, until the point just before the initial markers start to merge with each other (15). Jung and Kim determine the h value that optimizes an evaluation function in an iterative algorithm (16). However, once they fix the h values, these algorithms use them for the entire image/component. Our proposed algorithm differs from these algorithms in the sense that it identifies its markers using multiple h values for the same image/component. By doing so, it alleviates the over and undersegmentation problems due to the use of the same h value for the entire image/component. Our experiments on widefield fluorescence microscopy images demonstrate that this use of multiple h values improves the segmentation performance for nuclei of both isolated and confluent cells.

In our previous studies (18,19), we also developed marker-controlled watershed algorithms. However, as opposed

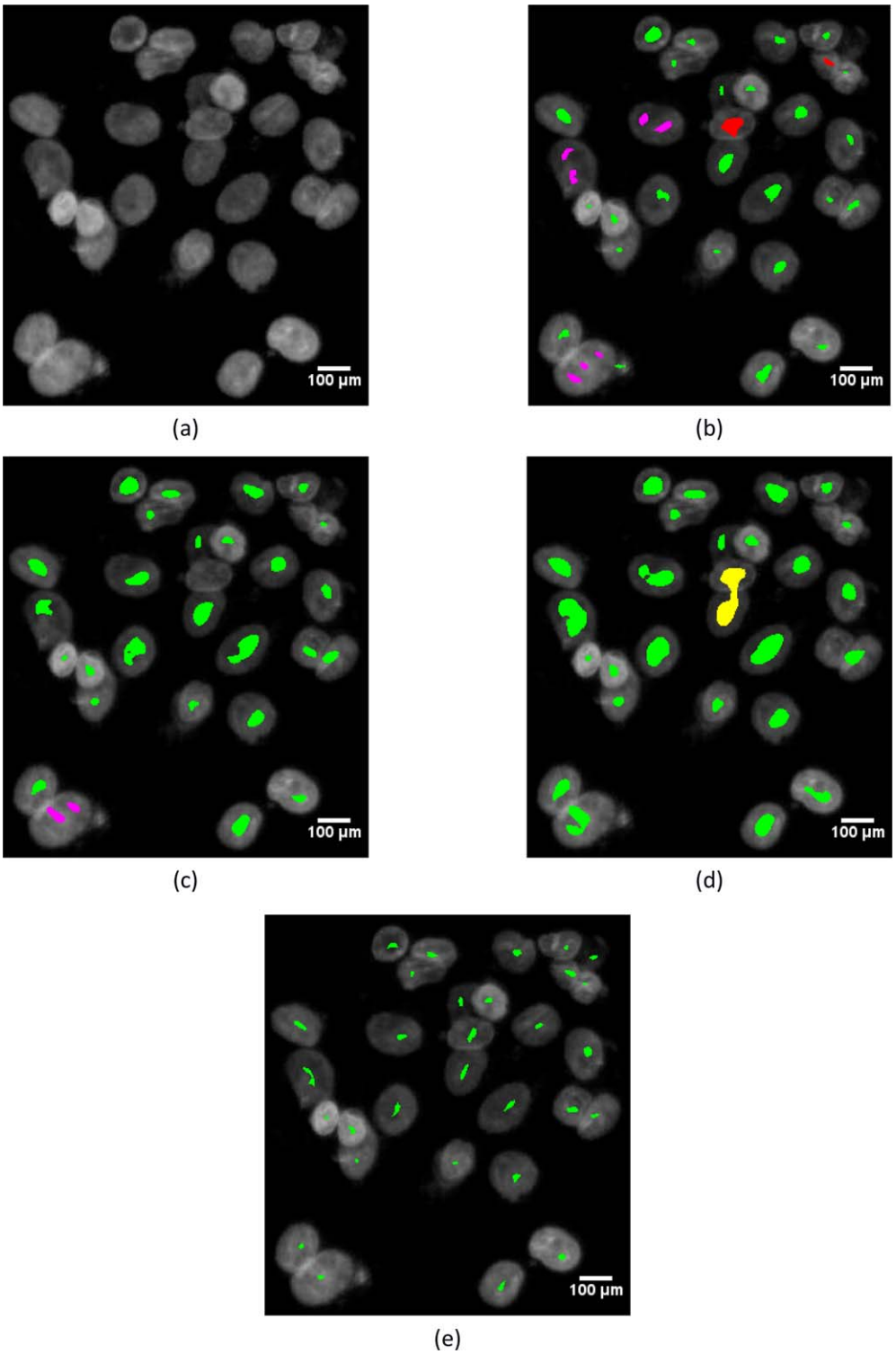

Figure 2. Markers found on an example subimage: (**a**) original subimage, (**b**) markers when $h = 1$, (**c**) markers when $h = 2$, and (**d**) markers when $h = 3$. Here, magenta and yellow markers indicate oversegmentations and undersegmentations, respectively. The markers that cannot be identified with larger h values are shown with red in (b). The markers identified by our proposed algorithm are shown in (**e**). [Color figure can be viewed in the online issue, which is available at wileyonlinelibrary.com.]

to this current work, in (18), we determined the markers using the h-minima transform with a fixed h value. In (19), we defined the markers using intensity and gradient properties of the live cells specific to the KATO-3 cell line; we did not use the h-minima transform at all. Different than these watersheds, in (20), we developed a model-based segmentation algorithm that

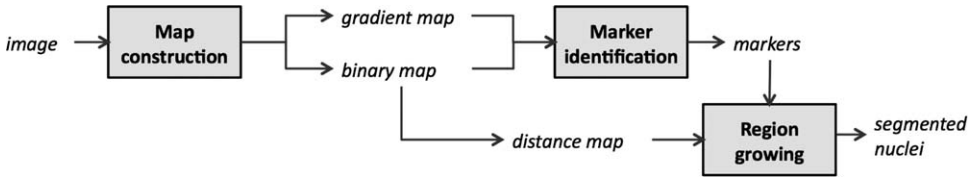

Figure 3. Schematic overview of our proposed algorithm.

identifies the initial nucleus locations using a graphical model constructed on nucleus boundaries and grows them also using these boundaries. In this current work, we point to the problem of using a single fixed h value to identify the markers of all nuclei within the same image/component and propose a new iterative h-minima-based watershed algorithm that uses multiple h values for more accurate cell nucleus segmentation.

Methodology

Our proposed algorithm relies on using multiple h values to identify the markers of a connected component, which corresponds to a nucleus clump in an image. The motivation behind this use is the fact that there exists no best h value that can be used to identify all markers of the same connected component, due to the possible variations in the nuclei's sizes, shapes, and intensities within the same nucleus clump. Our algorithm has three main steps: map construction, marker identification, and region growing.[1] The schematic overview of the algorithm is given in Figure 3. The details of its steps are given in the following subsections.

Map Construction

In this step, we construct two maps on which initial markers are identified and grown. These are the gradient map G_{map}, which we use to model the intensity deviations along the nucleus boundaries, and the distance transform map D_{map}, which we use to model the size and shape of nuclei.

For an image I, we obtain the gradient map G_{map} by applying the Sobel operators on its grayscale. Here we smooth both the grayscale image and the Sobel responses to reduce intensity variations and noise within nuclei. In particular, before applying the Sobel operators, we smooth the grayscale image by morphological opening that uses a disk structuring element with a radius of d_{size}. Then, after obtaining them, we smooth the Sobel responses using the average filter also with a half size of d_{size}. Note that we select the diameter (radius) of the disk structuring element and the filter size (its half size) the same to reduce the number of free model parameters in our algorithm.

We calculate D_{map} by taking the distance transform for the pixels of a binary mask B, which is obtained by thresholding the grayscale of the image I. In our algorithm, we use a global threshold value calculated by the Otsu's method (21). However, we use its half to ensure that the mask covers most of the nuclear regions.

Iterative Marker Identification

Watershed-based nucleus segmentation algorithms commonly define their markers on nucleus centroids. For that, they typically find regional maxima on a distance transform map, to reflect a fact that nucleus centroids are the locations farthest from boundaries, and/or regional minima on a gradient map, to reflect a fact that the centroids typically show smallest intensity deviations. In this work, we use the gradient map G_{map} to iteratively identify the markers. In each iteration of this process, we first suppress noise on G_{map} using the h-minima transform, with a different h value, and then find the regional minima on the noise-suppressed map. The motivation behind using different h values in different iterations is that the selection of the h value is not straightforward since a single fixed h value would not be enough to suppress all noise at a desired level, and thus, different h values work with different levels of success to identify the markers corresponding to different types of nuclei. Smaller h values work better to identify the correct markers for nuclei containing a fair amount of noise inside, but may yield oversegmented markers for those with a high amount of noise. On the other hand, larger h values address the oversegmentation problem, but this time, they may lead to undersegmented or missing markers for the former type of nuclei. Thus, in order to address this problem, we proposed to use multiple h values in an iterative algorithm (see Fig. 2).

In this algorithm, we start iterations from $h = 1$ and increment its value by one until no new markers are defined. In each iteration, we suppress noise on G_{map} using the h-minima transform and identify the regional minima on the noise-suppressed map as marker candidates. Then, in order to reduce the number of oversegmented markers, whose areas are typically small especially when a small h value is used, we eliminate the candidates that are smaller than an area threshold t_{area}. We eliminate such small candidates to prevent defining a noisy region as a marker. Note that if such a region corresponds to a true marker, next iterations are expected to locate it since larger h values typically yield larger candidates (regional minima).

At the end, we add the candidates to the marker set provided that they do not overlap with the markers defined in the previous iterations. Here instead of considering the previous markers as they are, we dilate them with a disk structuring element, whose radius is also d_{size}, and determine the overlaps accordingly. The rationality of this dilation is that consecutive

[1]We implement the map construction and marker identification steps in Matlab, using its built-in function for h-minima transform. We implement the region growing step in C. The source codes of our implementation are available at http://www.cs.bilkent.edu.tr/~gunduz/downloads/IterativeHMin.

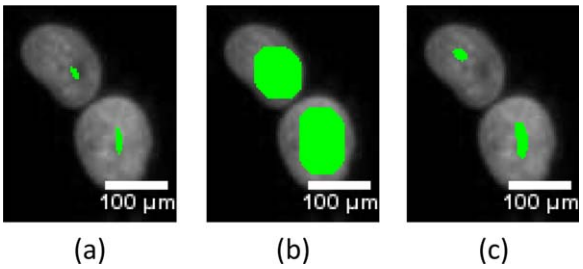

Figure 4. (**a**) Previously identified markers before dilation, (**b**) previously identified markers after dilation, and (**c**) currently identified markers. There is no overlap between the top marker of (a) and the top marker of (c) before dilation. However, after dilation, these two become overlapping and the top marker of (c) will not be included into the marker set, which prevents oversegmentation for the top nucleus. [Color figure can be viewed in the online issue, which is available at wileyonlinelibrary.com.]

h values may yield overlapping markers or those that are not overlapping but very close to each other and the dilation prevents oversegmentation arising from such close markers (see Fig. 4).

Algorithm 1. ITERATIVE MARKER IDENTIFICATION
Input: gradient map G_{map}, area threshold t_{area}, disk size d_{size}
Output: markers M
$M = \varnothing$
$h = 1$
repeat
$h_{\text{map}} \leftarrow$ H-MINIMA (G_{map}, h)
$M_{\text{curr}} \leftarrow$ REGIONAL MINIMA (h_{map})
$M_{\text{curr}} \leftarrow$ ELIMINATE SMALL (M_{curr}, t_{area})
$M_{\text{curr}} \leftarrow$ ELIMINATE OVERLAPPING (M, M_{curr}, d_{size})
$M = M \cup M_{\text{curr}}$
$h = h + 1$
until $\boldsymbol{M_{\text{curr}} = \varnothing}$

We provide the pseudocode of this iterative marker identification in Algorithm 1. This algorithm takes three inputs. The first one is the gradient map G_{map}, on which markers are identified. The next one is the area threshold t_{area}, which is used to eliminate small marker candidates. The last input is the radius d_{size} of a disk structuring element, which is used to dilate the previous markers for determining the overlaps. The iterative marker identification algorithm outputs the marker set M. Figure 5 illustrates an example output of this algorithm, each iteration of which uses a different h value. Each image shown in this figure corresponds to a different iteration and illustrates the markers added to the marker set in the current iteration in red and those found in the previous iterations in green.

Region Growing

After identifying the markers, we grow the dilated markers on the foreground pixels of the binary mask B by a marker-controlled watershed algorithm and delineate the nucleus boundaries. We use the distance transform map D_{map} as the marking function in the flooding process of the watershed. For each foreground pixel, D_{map} keeps the closest distance from this pixel to its closest marker. In a standard watershed algorithm, the flooding process grows the identified markers on all foreground nucleus pixels until the grown markers meet. However, this may cause a problem when markers are not correctly identified for all adjacent nuclei. Figure 6 illustrates this problem on two subimages, each of which contains three nuclei. In each subimage, the markers are correctly identified for the two nuclei but no marker is found for the other nucleus (Fig. 6a). The standard flooding process grows these markers on the nucleus pixels, whose boundaries are given in Figure 6b. Thus, it yields incorrect nucleus boundaries, as shown in Figure 6c, since some of these pixels belong to the nucleus with an unidentified marker.

To prevent flooding into pixels that belong to a nucleus with an unidentified marker, we modify the flooding process such that it grows a marker on a foreground pixel unless it meets the stopping condition for this pixel, which is defined considering other pixels found in its symmetric location. Particularly, to grow a marker M on a foreground pixel P, we check all pixels found on a circular arc, whose midpoint is symmetric to P with respect to the M's centroid. The start and end angles of the arc are $-\alpha$ and $+\alpha$ degrees with respect to the line passing through this midpoint and the M's centroid (see Fig. 7). We allow growing only if none of the pixels on this arc belong to the background or have previously been assigned to another marker. At the end, when none of the markers can be grown further, we allow them to grow on the foreground at most p more pixels without considering the stopping condition. For the subimages given in Figure 6a, the boundaries obtained by our modified flooding process are shown in Figure 6d. Note that since this flooding process considers pixels on an arc, instead of an entire circle, it locates non-circular nuclei better, as illustrated in Figure 8.

Experiments

Dataset

In our experiments, we use fluorescence microscopy images of human hepatocellular carcinoma (Huh7 and HepG2) cell lines that were cultured in the Molecular Biology and Genetics Department at Bilkent University. The cells were stained with Hoechst 33258 nuclear staining and their images were taken under a Zeiss Axioscope fluorescent microscope with an AxioCam MRm monochrome camera. The objective lens is 20× and the image size is 768 × 1,024. The cell nuclei in these images were annotated by our biologist collaborators.

First, we conduct experiments on the dataset that we used in our previous work (20). In this dataset, 785 nuclei are used as training instances, on which the parameters of the algorithms are selected. These nuclei are taken from 10 randomly selected images; five of them are selected from the Huh7 cell line and the other five from the HepG2 cell line. The rest of the images are used as test instances. Since cells are grown in more overlayers in the HepG2 cell line and since we want to explore the effectiveness of the algorithms on different confluency levels, there are two test sets. The first one contains

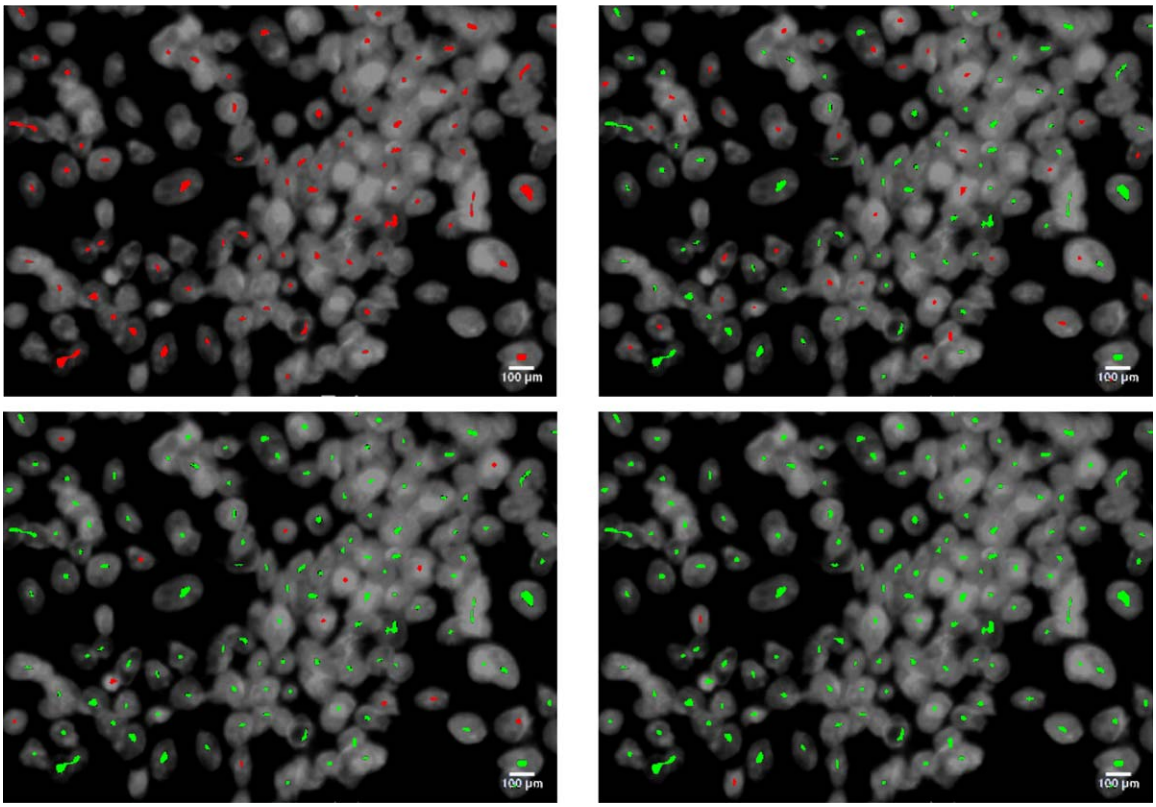

Figure 5. Outputs of four different iterations, each of which uses a different *h* value, in the marker identification step. In each image, the red markers are the ones that are added to the marker set in the current iteration and the green markers are those that were found in the previous iterations. [Color figure can be viewed in the online issue, which is available at wileyonlinelibrary.com.]

891 nuclei taken from 11 images of the Huh7 cell line. The second one contains 985 nuclei taken from 16 images of the HepG2 cell line. In addition to these test sets, which were taken from our previous work (20), we form another one that contains more confluent cells. This test set contains 1,065 nuclei taken from 4 images of the HepG2 cell line. We will refer them as the Huh7 test set, the HepG2 test set, and the dense HepG2 test set, respectively.

Evaluation

We evaluate our proposed algorithm and the comparison methods, both visually and quantitatively. For quantitative

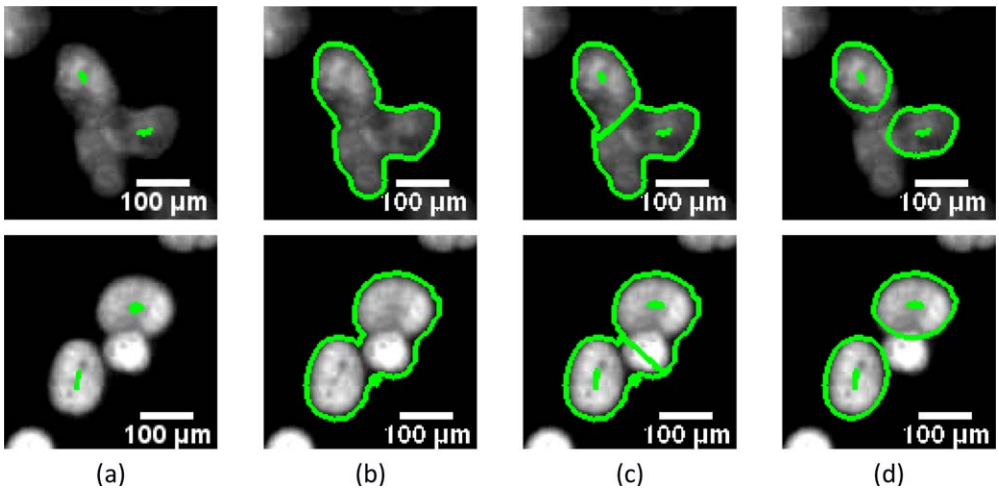

Figure 6. Flooding process of the watershed algorithm for two example subimages. (**a**) Markers from which flooding starts, (**b**) boundaries of nucleus pixels, (**c**) nucleus boundaries obtained using the standard flooding process, (**d**) nucleus boundaries obtained using our flooding process. [Color figure can be viewed in the online issue, which is available at wileyonlinelibrary.com.]

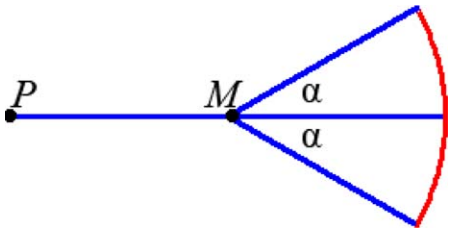

Figure 7. Illustration of defining the stopping condition in region growing. To grow a marker *M* on a pixel *P*, this condition checks all pixels (red pixels in this figure) on a circular arc, whose midpoint is symmetric to *P* with respect to the *M*'s centroid. [Color figure can be viewed in the online issue, which is available at wileyonlinelibrary.com.]

evaluation, we use the precision, recall, and *F*-score metrics. First, we calculate these metrics on nuclei to quantify how successful an algorithm is in the correct identification of nuclei. Then, we calculate them on pixels by considering the correctly segmented pixels of only the correctly identified nuclei as correct segmentation.

We determine the correctly identified nuclei as follows. We match each nucleus *N* that an algorithm segments with an annotated nucleus *A* in the gold standard if at least half of *N*'s segmented pixels overlap with those of *A*. Likewise, we match each annotated nucleus with a segmented nucleus. Then, *N* is considered as correctly identified if there is a one-to-one match between *N* and an annotated nucleus. Otherwise; (1) *N* is a false detection if it does not match with any annotated nuclei, (2) *A* is a miss if it does not match with any segmented nuclei, (3) *A* is oversegmented if more than one segmented nucleus match with *A*, and (4) annotated nuclei that match with the same segmented nucleus are undersegmented.

Parameter Selection

The proposed algorithm has four external parameters. The first one is the area threshold t_{area}, which is used to eliminate smaller markers in the marker identification step. The second parameter d_{size} is used in two different steps: map construction and marker identification. In the map construction step, it determines the size of the disk structuring element and the average filter, both of which are used for smoothing operation. In the marker identification step, this parameter also determines the size of the disk structuring element, which is used to dilate the previous markers for eliminating the overlapping markers. Note that although it is possible to use different values, we set the radius of the disk structuring elements and the half size of the average filter to the same d_{size} value to reduce the number of the external parameters of our algorithm. The last two parameters are used in the region growing step. The angle α is used to define the start and end points of an arc, whose pixels are used to define the stopping condition of the flooding process. The offset p is the maximum number of pixels that a marker grows at the end without considering the stopping condition. In our experiments, we consider any combination of the following values $t_{area} = \{5, 10, 20, 30\}$, $d_{size} = \{5, 7, 10, 13\}$, $\alpha = \{0, 15, 30, 45\}$, and $p = \{0, 2, 4\}$, and select the one that maximizes the *F*-score metric on the training set. The selected parameter values are $t_{area} = 20$, $d_{size} = 10$, $\alpha = 15$, and $p = 2$. In this selection, none of the test set images are used.

In addition to these external parameters, we have an internal choice, which is the decrease ratio of the Otsu threshold to obtain the binary mask *B* in the map construction step. In this step, we decrease the Otsu threshold to its half (i.e., use the 0.5 ratio) to ensure that *B* covers most of the nucleus pixels. We will analyze the effects of this selection to the segmentation performance in Analyses section.

Comparisons

We compare our proposed algorithm with four nucleus segmentation methods: adaptive h-minima (15), conditional erosion (22), iterative voting (10), and ARGraphs (20). The first two are marker-controlled watersheds. The adaptive h-minima method (15) identifies markers by finding regional minima on the inverse distance map. It also uses the h-minima transform to suppress noise on the distance map. After selecting a *h* value and identifying the markers, it adaptively changes this *h* value to obtain better shaped markers. Different than the one used by our proposed algorithm, this adaptive method affects only the shape of the markers, all of which are found using the same *h* value. The conditional erosion method (22) finds its markers by iteratively eroding the binary mask of an image using two different structuring elements.

The other two are model-based segmentation algorithms. The iterative voting method (10) gets image pixels iteratively voted along the radial and tangential directions to determine nucleus centers. The ARGraphs (20) method, which we previously implemented in our research group, models nucleus boundaries by an attributed relational graph and identifies nucleus centers by searching patterns on this graph. Once they identify the nucleus centers, both of these methods delineate nuclei, growing the centers by a watershed algorithm. Note that we select the parameters of these four comparison methods also on the training set images.

Results

We provide the quantitative results of our algorithm and the comparison methods in Figure 9 and report their nucleus-based *F* score metrics in Table 1; the detailed results are given in the supplementary material (23). The figure and the table

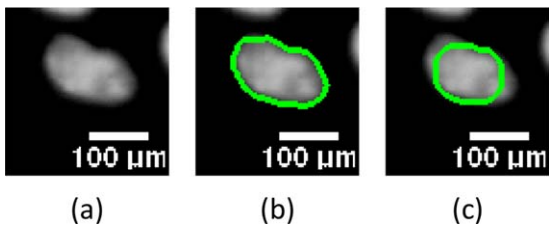

Figure 8. Effects of defining the stopping condition by considering the pixels of an arc instead of an entire circle. (**a**) An example image of nucleus, (**b**) boundaries obtained when the pixels of an arc are considered, and (**c**) boundaries obtained when the pixels of an entire circle are considered. [Color figure can be viewed in the online issue, which is available at wileyonlinelibrary.com.]

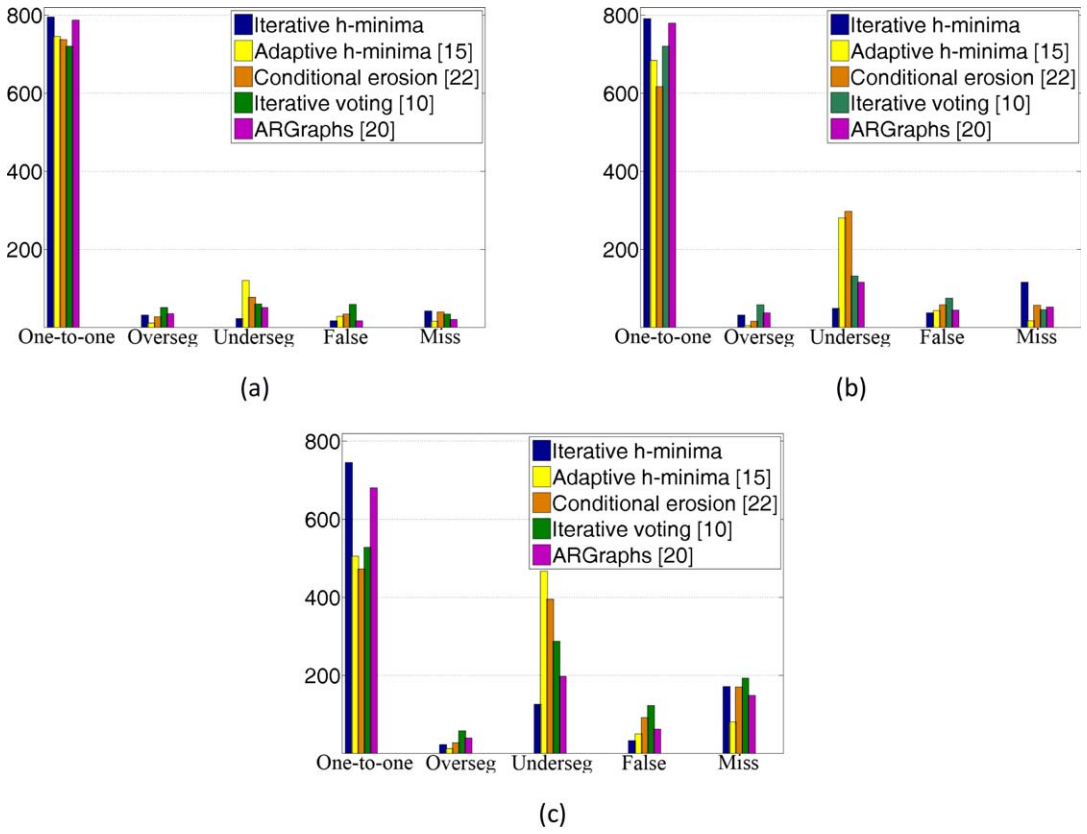

Figure 9. Comparison of the algorithms in terms of segmented-annotated nucleus matches on the (**a**) Huh7, (**b**) HepG2, and (**c**) dense HepG2 test sets. [Color figure can be viewed in the online issue, which is available at wileyonlinelibrary.com.]

show that the proposed algorithm improves the segmentation performance of the other methods. This improvement is more evident in more confluent cells, as seen in the results obtained on the dense HepG2 test set (Fig. 9c and the fourth column of Table 1). These quantitative results are also consistent with the visual ones given in Figure 10. The first two rows of this figure contain subimages taken from the Huh7 test set, which typically have nuclei of isolated and less confluent cells. All algorithms give good segmentation results for almost all of such nuclei. The next two rows contain subimages from the HepG2 test set and the last two contain subimages from the dense HepG2 test set. These visual results show that as the confluency degree increases, the performance of the comparison methods decreases more compared to our proposed algorithm.

Table 1. Comparison of the algorithms in terms of nucleus-based *F* score measures on the Huh7, HepG2, and dense HepG2 test sets

	HUH7	HEPG2	DENSE HEPG2
Iterative h-minima	89.29	83.22	76.59
Adaptive h-minima (15)	85.87	74.50	57.05
Conditional erosion (22)	84.01	67.80	51.64
Iterative voting (10)	81.10	74.52	53.63
ARGraphs (20)	88.29	80.28	68.75

The comparison between our proposed algorithm and the adaptive h-minima method also reveals that using multiple h values to identify the markers for the same connected component leads to better segmentation results. To investigate whether this is indeed a result of using multiple values or improper selection of the fixed h value, we conduct another experiment. For that, we have modified our algorithm such that it uses a single fix h value; the other parts of the algorithm remain exactly the same. For the Huh7, HepG2, and dense HepG2 test sets, Figure 11 shows the nucleus based F score metric as a function of h values. For each test set, it also plots the nucleus based F-score metric obtained by our proposed algorithm, which iteratively uses multiple h values. This figure shows that it is possible to obtain a similar F score metric when the optimal h value is used for the Huh7 test set, in which cell nuclei are isolated or less confluent (Fig. 11a). On the other hand, the gap between the F scores obtained by the proposed algorithm and the optimal h value increases for the HepG2 and dense HepG2 test sets, in which cell nuclei are more confluent. This indicates the effectiveness of using multiple h values, especially when cell nuclei form denser clusters.

Analyses

Our proposed algorithm has four external parameters: the area threshold t_{area}, the size d_{size} of the disk structuring elements and the average filter, the angle α, and the offset p. As explained in Parameter Selection section, we select the values

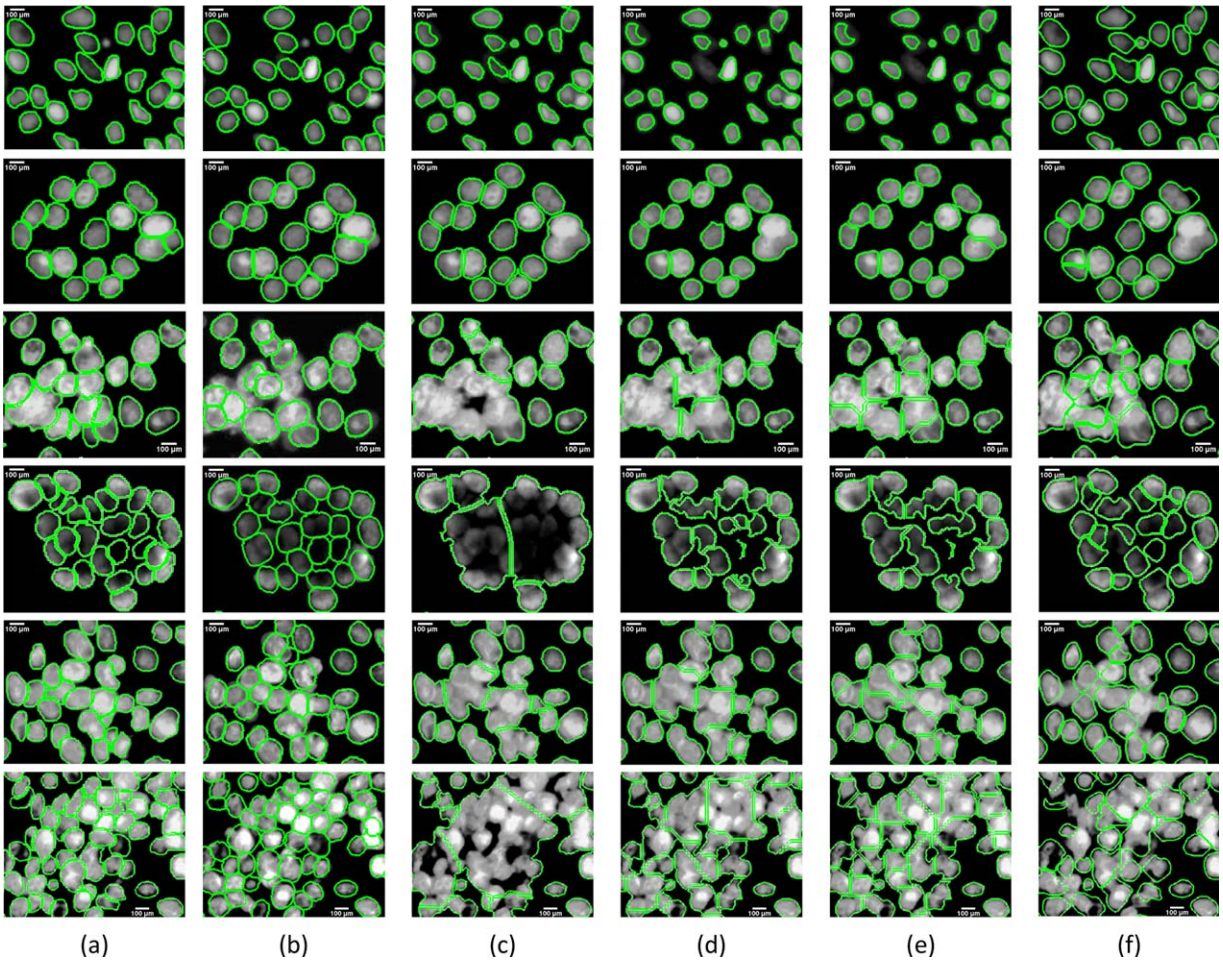

Figure 10. Visual results for various subimages: (**a**) annotated nuclei in the gold standard, (**b**) results by the proposed iterative h-minima algorithm, (**c**) results by the adaptive h-minima method (15), (**d**) results by the conditional erosion method (22), (**e**) results by the iterative voting method (10), and (**f**) results by the ARGraphs method (20). The first two rows contain subimages from the Huh7 test set, the next two contain subimages from the HepG2 test set, and the last two contain the subimages from the dense HepG2 test set. Note that the subimage sizes have been scaled for better visualization. [Color figure can be viewed in the online issue, which is available at wileyonlinelibrary.com.]

of these parameters on the training set, without using any test set images at all. Besides, the algorithm has an internal choice, which is the Otsu threshold ratio. Although this ratio could also be considered as an external parameter and its value could also be selected on the training set, we fix it to 0.5 for reducing the number of free model parameters in our algorithm. In this section, we will first analyze the effect of this choice to the segmentation results.

To identify the foreground pixels, we obtain a binary mask B by thresholding the grayscale image. Here we calculate the threshold value by the Otsu's method (21) and decrease this value to its half to ensure that the mask covers most of the nucleus pixels. However, instead of decreasing the value to its half (i.e., using the 0.5 ratio), it is also possible to use other decrease ratios. In Figure 12, we analyze the effects of using different Otsu threshold ratios to the F score metrics for the three test sets used in our experiments. This figure indicates that ratios in the range of 0.4 and 0.8 give similar results and the segmentation performance does not very much depend on a specific value of this ratio.

Next, we analyze the effects of image quality degradation to segmentation results. To this end, we degrade the quality of images by blurring them with a Gaussian filter and added Poisson noise to the blurred image. Figure 13 shows the F score metric as a function of the standard deviation σ of the Gaussian filter, which controls the degradation degree. This figure shows that our proposed algorithm is robust to image quality degradation to a certain extent. However, as expected, when the image quality drops below a certain point (when the standard deviation σ too much increases), there is a substantial decrease in the segmentation performance.

Experiments on Tissue Section Images

In our experiments, we test our proposed algorithm on the images of cultured human hepatocellular carcinoma (Huh7 and HepG2) cell lines. To understand its applicability on different image types, we extend the application of our algorithm on images of tissue sections from mouse liver, which were stained with 4',6-diamidino-2-phenylindole (DAPI) nuclear stain. The images of these tissue sections were taken under a fluorescent

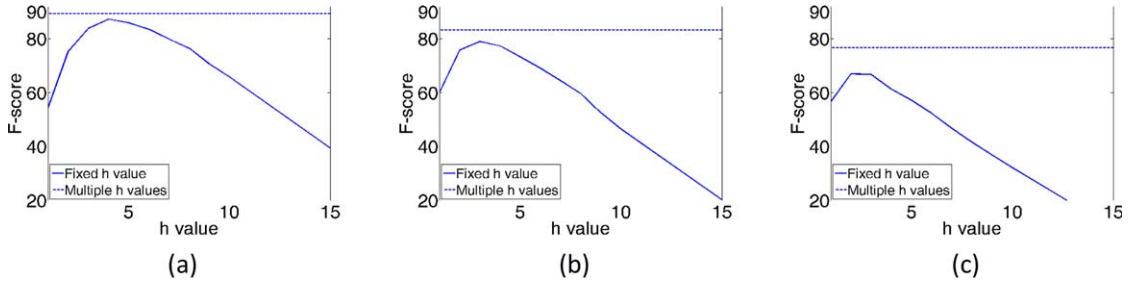

Figure 11. Nucleus based *F* score metrics obtained when a fixed *h* value is used (solid lines) and when multiple *h* values are iteratively used by our proposed algorithm (dashed lines). The *F* score metrics are obtained for the (**a**) Huh7, (**b**) HepG2, and (**c**) dense HepG2 test sets. [Color figure can be viewed in the online issue, which is available at wileyonlinelibrary.com.]

microscope with a 20× objective lens. The image size is 480 × 640. Our biologist collaborators annotated these images by marking the cell nuclei without drawing their boundaries. Because these annotations do not include the nucleus boundaries but a marker for each nucleus, we consider a segmented nucleus as a one-to-one match if this nucleus contains only a single marker, which indicates a gold standard nucleus, inside. For quantitative evaluation, we compute the precision, recall, and *F* score metrics on these one-to-one matches.

In this tissue section dataset, there are a total of 13 images containing 2,660 cell nuclei. Because these images may show characteristics different than those of cultured human hepatocellular carcinoma cell lines, we randomly separate them into the training set (766 nuclei from four images) and the test set (1,894 nuclei from the remaining nine images) and select the model parameters again on the training nuclei. In this selection, we consider any combination of the following parameter values $t_{\text{area}} = \{5, 10, 15, 20, 30\}$, $d_{\text{size}} = \{3, 5, 7, 10, 13\}$, $\alpha = \{0, 15, 30, 45\}$, and $p = \{0, 2, 4\}$, and select the one that maximizes the *F*-score metric on the training nuclei. The selected parameter values are $t_{\text{area}} = 15$, $d_{\text{size}} = 5$, $\alpha = 30$, and $p = 2$. Likewise, we select the parameters of the comparison methods again, considering the training set of these tissue sections.

On the test set nuclei, our proposed algorithm gives 86.34% *F* score metric, leading to the highest *F* score compared to the other methods. The test set *F* scores are 78.65% for the adaptive h-minima method (15), 80.75% for the conditional erosion method (22), 78.49% for the iterative voting method (10), and 81.49% for the ARGraphs method (20); similarly, the detailed results are given in the supplementary material (23). We also present the visual results obtained on three example subimages in Figure 14. These preliminary results indicate that the proposed algorithm has a potential to be applied on other image types as well. One could consider the detailed investigation of this application as a future research direction of the proposed segmentation algorithm.

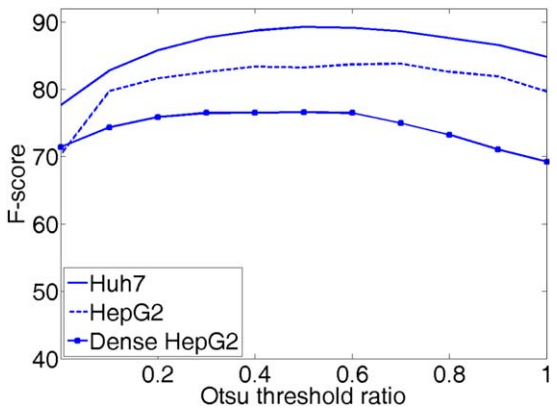

Figure 12. For the Huh7, HepG2, and dense HepG2 test sets, the nucleus-based *F* score metrics as a function of the Otsu threshold ratio used to obtain the binary mask.

Tight Nucleus Cluster Detection

Some images may contain tight clusters of nuclei, which cannot accurately be analyzed even manually. To identify such kind of clusters, we develop a simple detection algorithm, which determines markers whose likelihood of corresponding to nuclei in a tight cluster is high and eliminates these markers before region growing takes place. To this end, for each identified marker *M*, we calculate the minimum distance from its centroid to the background and the distance to the closest marker's centroid. We eliminate the marker *M* if both of these distances are greater than the distance threshold. The motivation behind using this method is the following. For a tight cluster that contains indiscernible nucleus boundaries, the

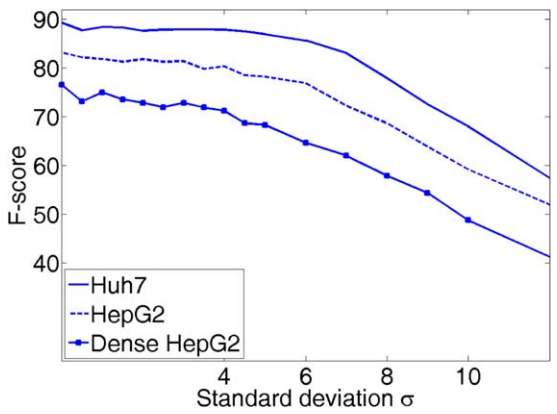

Figure 13. Effects of image quality degradation to segmentation results. For the Huh7, HepG2 and dense HepG2 test sets, the nucleus-based *F* score metrics as a function of the standard deviation σ of a Gaussian filter, with which images are blurred. Note that Poisson noise is also added to each blurred image.

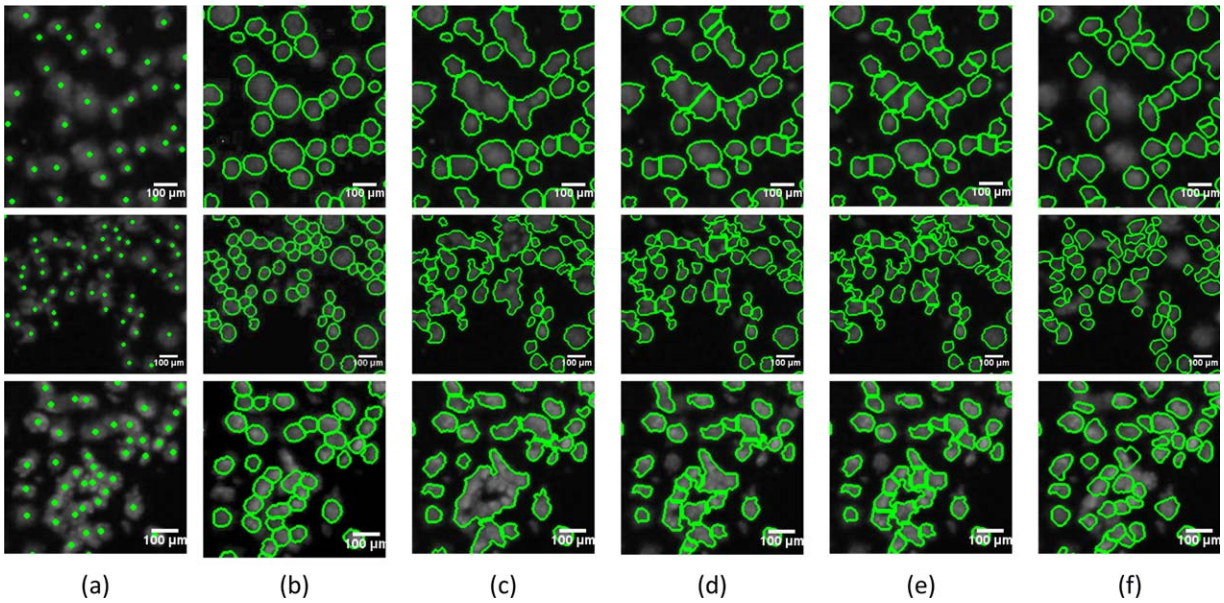

Figure 14. Visual results for various tissue section subimages: (**a**) annotated nuclei in the gold standard, (**b**) results by the proposed iterative h-minima algorithm, (**c**) results by the adaptive h-minima method (15), (**d**) results by the conditional erosion method (22), (**e**) results by the iterative voting method (10), and (**f**) results by the ARGraphs method (20). Note that the subimage sizes have been scaled for better visualization. [Color figure can be viewed in the online issue, which is available at wileyonlinelibrary.com.]

gradient map is not too much informative. As a result, only a few correct markers can be found within this tight cluster. Additionally, since such a cluster is typically large in size, these markers are usually far from the background.

In our experiments, we select the distance threshold as 30 considering the average radii of cell nuclei in the training images. As expected, the proposed tight nucleus cluster detection method does not eliminate any markers from the Huh7 test set since this set contains relatively less confluent cells. On the other hand, it eliminates one marker from the HepG2 and six markers from the dense HepG2 test sets, which contain more cells grown in overlayers. For an example subimage, taken from the dense HepG2 test set, the segmentation results obtained with and without using this detection method are given in Figure 15. As seen in this figure, no nuclei are found within the tight cluster of this subimage since the corresponding markers have been eliminated by the proposed detection method. Please note that the use of this method slightly changes the *F*-score metrics for the HepG2 sets; it changes the *F* scores from 83.22 to 83.16% for the HepG2 test set, and from 76.59 to 76.31% for the dense HepG2 test set.

Conclusion and Discussion

This article presents a new marker-controlled watershed algorithm for cell nucleus segmentation in fluorescence microscopy images. In this algorithm, we propose to define the markers iteratively, using a different *h* value in each iteration. The use of different *h* values suppresses noise at different levels, allowing us to define better markers for nuclei showing different characteristics. Our experiments on widefield fluorescence microscopy images demonstrate that this algorithm gives better markers for nuclei of both isolated and confluent cells, leading to better segmentation results.

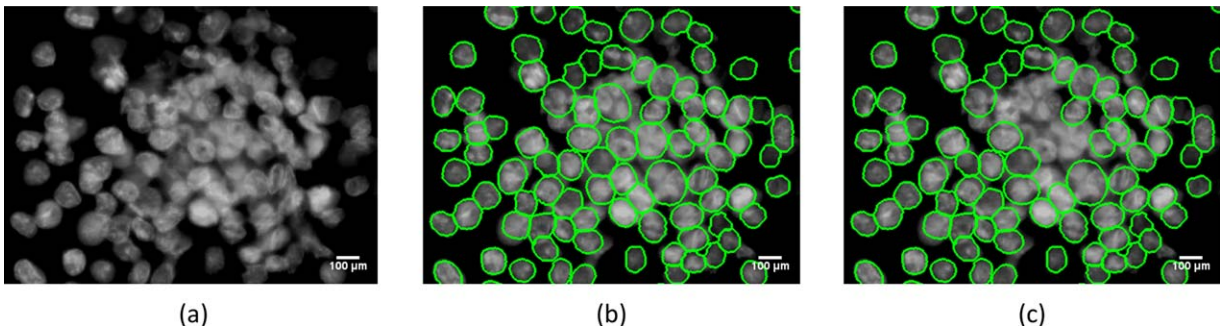

Figure 15. Visual segmentation results obtained when the tight nucleus cluster detection method is used. (**a**) Original subimage from the dense HepG2 test set, (**b**) nucleus boundaries obtained when the detection method is not used, and (**c**) nucleus boundaries obtained when the detection method is used. [Color figure can be viewed in the online issue, which is available at wileyonlinelibrary.com.]

In this work, we develop an algorithm for segmenting nuclei of both isolated and confluent cell taken from conventional widefield fluorescent microscopes, which are highly available and affordable for various laboratories. They are found in every molecular biology laboratory as well as they are routinely used for morphological analysis of cells in pathology diagnostics laboratories. However, we do not focus on confocal microscopy, which produces cell images with higher magnification and resolution for detailed visualization of subcellular distribution of fluorescent-labeled proteins. Although our algorithm can also be used for confocal microscopy images, simpler segmentation techniques would also be adequate for their segmentation since these images have only a few cells that are of higher magnification and resolution and that are mostly isolated (nonconfluent). However, the confocal microscopes may not be affordable for every research laboratory. Moreover, the interest may be the confluent cells if a researcher aims to see the aggregation of cells (e.g., cancer stem cell mammosphere formation). In such cases, our proposed algorithm can be used for cell nuclei segmentation.

We conduct our experiments on the images of cultured human hepatocellular carcinoma (Huh7 and HepG2) cell lines. To understand the applicability of our proposed algorithm on different image types, we also extend the application of our algorithm on images of tissue sections from mouse liver and obtain the preliminary results. The application of our algorithm on other image types could be considered as a future work.

In this work, we mainly focus on finding better markers. We use a relatively simple region growing algorithm to delineate nucleus boundaries. As another future work, we plan to work on designing better techniques for marker growing. Here one could consider designing iterative methods also in the region growing process. Another possibility is to explore the use of other types of maps, on which the growing takes place.

Literature Cited

1. Chen X, Zhou X, Wong ST. Automated segmentation, classification, and tracking of cancer cell nuclei in time-lapse microscopy. IEEE Trans Biomed Eng 2006;53:762–766.
2. Kharma N, Moghnieh H, Yao J, Guo YP, Abu-Baker A, Laganiere J, Rouleau G, Cheriet M. Automatic segmentation of cells from microscopic imagery using ellipse detection. IET Image Proc 2007;1:39–47.
3. Dima AA, Elliott JT, Filliben JJ, Halter M, Peskin A, Bernal J, Kociolek M, Brady MC, Tang HC, Plant AL. Comparison of segmentation algorithms for fluorescence microscopy images of cells. Cytometry A 2011;79A:545–559.
4. Fenistein D, Lenseigne B, Christophe T, Brodin P, Genovesio A. A fast, fully automated cell segmentation algorithm for high-throughput and high-content screening. Cytometry A 2008;73:958–964.
5. Yang F, Jiang T. Cell image segmentation with kernel-based dynamic clustering and an ellipsoidal cell shape model. J Biomed Inform 2001;34:67–73.
6. Jung C, Kim C, Chae SW, Oh S. Unsupervised segmentation of overlapped nuclei using Bayesian classification. IEEE Trans Biomed Eng 2010;57:2825–2832.
7. Plissiti M, Nikou C. Overlapping cell nuclei segmentation using a spatially adaptive active physical model. IEEE Trans Image Process 2012;21:4568–4580.
8. Kumar S, Ong SH, Ranganath S, Ong TC, Chew FT. A rule-based approach for robust clump splitting. Pattern Recognit 2006;39:1088–1098.
9. Farhan M, Yli-Harja O, Niemisto A. A novel method for splitting clumps of convex objects incorporating image intensity and using rectangular window-based concavity point-pair search. Pattern Recognit 2013;46:741–751.
10. Parvin B, Yang Q, Han J, Chang H, Rydberg B, Barcellos-Hoff MH. Iterative voting for inference of structural saliency and characterization of subcellular events. IEEE Trans Image Process 2007;16:615–623.
11. Qi X, Xing F, Foran DJ, Yang L. Robust segmentation of overlapping cells in histopathology specimens using parallel seed detection and repulsive level set. IEEE Trans Biomed Eng 2012;59:754–765.
12. Hongming X, Cheng L, Mandal M. An efficient technique for nuclei segmentation based on ellipse descriptor analysis and improved seed detection algorithm. IEEE J Biomed Health Inform 2014;18:1729–1741.
13. Zhou X, Li F, Yan J, Wong ST. A novel cell segmentation method and cell phase identification using Markov model. IEEE Trans Inf Technol Biomed 2009; 13:152–157.
14. Wahlby C, Sintorn IM, Erlandsson F, Borgefors G, Bengtsson E. Combining intensity, edge and shape information for 2d and 3d segmentation of cell nuclei in tissue sections. J Microsc 2004;215:67–76.
15. Cheng J, Rajapakse JC. Segmentation of clustered nuclei with shape markers and marking function. IEEE Trans Biomed Eng 2009; 56:741–748.
16. Jung C, Kim C. Segmenting clustered nuclei using h-minima transform-based marker extraction and contour parameterization. IEEE Trans Biomed Eng 2010;57: 2600–2604.
17. Raimondo F, Gavrielides MA, Karayannopoulou G, Lyroudia K, Pitas I, Kostopoulos I. Automated evaluation of Her-2/neu status in breast tissue from fluorescent in situ hybridization images. IEEE Trans Image Process 2005; 14:1288–1299.
18. Arslan S, Ozyurek E, Gunduz-Demir C. A color and shape based algorithm for segmentation of white blood cells in peripheral blood and bone marrow images. Cytometry A 2014; 85A:480–490.
19. Koyuncu CF, Arslan S, Durmaz I, Cetin-Atalay R, Gunduz-Demir C. Smart markers for watershed-based cell segmentation. PloS One 2012;7:e48664.
20. Arslan S, Ersahin T, Cetin-Atalay R, Gunduz-Demir C. Attributed relational graphs for cell nucleus segmentation in fluorescence microscopy images. IEEE Trans Med Imaging 2013;32:1121–1131.
21. Otsu N. A threshold selection method from gray-level histograms. IEEE Trans Sys Man 1979;9:62–66.
22. Yang X, Li H, Zhou X. Nuclei segmentation using marker-controlled watershed, tracking using mean-shift, and Kalman filter in time-lapse microscopy. IEEE Trans Circ Syst I 2006;53:2405–2414.
23. Koyuncu C, Akhan E, Cetin-Atalay R, Gunduz Demir C. Iterative h-minima based marker-controlled watershed for cell nucleus segmentation: Supplementary material. Computer Engineering, Bilkent University, Technical Report, BU-CE-1501, 2015 [Online]. Available at: http://www.cs.bilkent.edu.tr/tech-reports/2015/BU-CE-1501.pdf.